



ISTITUTO NAZIONALE DI RICERCA METROLOGICA Repository Istituzionale

Photon Statistics Modal Reconstruction by Detected and Undetected Light

Original

Photon Statistics Modal Reconstruction by Detected and Undetected Light / Knoll, Laura T.; Petrini, Giulia; Piacentini, Fabrizio; Traina, Paolo; Polyakov, Sergey V.; Moreva, Ekaterina; Degiovanni, Ivo Pietro; Genovese, Marco. - In: ADVANCED QUANTUM TECHNOLOGIES. - ISSN 2511-9044. - 6:8(2023).
[10.1002/qute.202300062]

Availability:

This version is available at: 11696/80240 since: 2024-03-04T09:16:32Z

Publisher:

WILEY

Published

DOI:10.1002/qute.202300062

Terms of use:

This article is made available under terms and conditions as specified in the corresponding bibliographic description in the repository

Publisher copyright

(Article begins on next page)

Photon Statistics Modal Reconstruction by Detected and Undetected Light

Laura T. Knoll, Giulia Petrini, Fabrizio Piacentini, Paolo Traina, Sergey V. Polyakov, Ekaterina Moreva, Ivo Pietro Degiovanni,* and Marco Genovese

A novel technique is introduced for the reconstruction of multimode optical fields, based on simultaneously exploiting both the generalized Glauber's K^{th} -order correlation function $g^{(K)}$ and a recently proposed anti-correlation function (dubbed $\theta^{(K)}$) which is resilient to Poissonian noise. It is experimentally demonstrated that this method yields mode reconstructions with higher fidelity with respect to those obtained with reconstruction methods based only on $g^{(K)}$'s, even requiring less "a priori" information. The reliability and versatility of this technique make it suitable for a widespread use in real applications of optical quantum measurement, from quantum information to quantum metrology, especially when one needs to characterize ensembles of single-photon emitters in the presence of background noise (due, for example, to residual excitation laser, stray light or unwanted fluorescence).

metrology^[6] up to a point where the associated techniques are not anymore restricted to scientific labs, but are starting to effectively proliferate to the industry^[7,8] and the world-wide market,^[9] ultimately approaching everyday's life. This much-awaited "second quantum revolution"^[10] paves the way for increasingly complex schemes to exploit the advantages of quantum effects for applications in practical scenarios such as quantum computation,^[7,11–16] quantum communication,^[1,17,18] quantum-enhanced measurement,^[19–24] quantum imaging and sensing,^[25–30] and quantum testing.^[31,32] As a consequence, it is of the utmost importance to develop simple methods^[33–39] to characterize optical states that are

significantly more complex than that of the proof-of-principle single isolated quantum systems (with possible addition of a small amount of background). Composite and application-driven quantum systems require an appropriate characterization. Such systems are significantly affected by inevitable noise and decoherence effects occurring when the system is moved from a controlled lab-like environment to a real-world one for a practical application. From a theoretical point of view, devising reliable and robust nonclassicality criteria for such quantum systems is a topic of high interest.^[40–42] For instance, the characterization of ensembles of single-photon sources (SPSs)^[43,44] in the presence of strong noise baths is considered. The most widespread techniques for the characterization of quantum optical states are based on the measurement of second order Glauber's autocorrelation function, defined as

$$g^{(2)}(\tau) = \frac{\langle E^{(-)}(t)E^{(-)}(t+\tau)E^{(+)}(t+\tau)E^{(+)}(t) \rangle}{\langle E^{(-)}(t)E^{(+)}(t) \rangle^2} \quad (1)$$

and in particular its $g^{(2)}(0)$ value.

This parameter is typically used to intuitively assess the non-classicality of optical sources, since its value is below one for sub-poissonian non-classical light, equal to one for a Poissonian (laser) source, and above one for other classical states. In particular, $g^{(2)}(0)$ vanishes for a SPS, being exactly 0 in the ideal case.^[45] In the low-photon-flux regime, that is, when $P(n+1) \ll P(n) \ll 1$ (being $P(n)$ the probability of observing n photons in our detector), this parameter is equivalent to Grangier's parameter α ,^[46] defined as the ratio between the photon coincidence probability and the product of the single photon detection probabilities at the output of a Hanbury–Brown & Twiss interferometer

1. Introduction

Recent years have seen an impressive advancement of quantum technology in the optical domain^[1–5] and single-photon

L. T. Knoll, G. Petrini, F. Piacentini, P. Traina, E. Moreva, I. P. Degiovanni, M. Genovese

INRIM

strada delle Cacce 91, Torinol-10135, Italy

E-mail: i.degiovanni@inrim.it

L. T. Knoll

DEILAP-UNIDEF, CITEDEF-CONICET

J.B. de La Salle 4397, 1603 Villa Martelli, Buenos AiresArgentina

G. Petrini

Physics Department – University of Torino

Via Pietro Giuria 1, Torinol-10126, Italy

S. V. Polyakov


National Institute of Standards and Technology

100 Bureau Drive, Gaithersburg, MD20899, USA

I. P. Degiovanni, M. Genovese

INFN

via P. Giuria 1, Torinol-10125, Italy

 The ORCID identification number(s) for the author(s) of this article can be found under <https://doi.org/10.1002/qute.202300062>

© 2023 The Authors. Advanced Quantum Technologies published by Wiley-VCH GmbH. This is an open access article under the terms of the Creative Commons Attribution-NonCommercial-NoDerivs License, which permits use and distribution in any medium, provided the original work is properly cited, the use is non-commercial and no modifications or adaptations are made.

DOI: 10.1002/qute.202300062

(HBTI), which is the typical device used to measure $g^{(2)}$ experimentally. This parameter ($g^{(2)}$ or α , with no distinction in the following treatment) can immediately be extended to any order K by defining $g^{(K)}$ as the ratio of the probability of a K -fold coincidence divided by the product of K single click probabilities of K non-photon-number-resolving (non-PNR) detectors attached to the output ports of a generalized multiport HBTI. Operationally, such an HBTI can be comprised of cascaded two-ports beam splitters.^[47–52] One of the main advantages of this parameter is that its value does not depend on the splitting ratio among the HBTI arms, on the overall losses and on the detection efficiency of the detectors comprising the HBTI.

The experimental measurement of $g^{(K)}$ has proven to be a useful resource in quantum optics for several applications ranging from SPS characterization, quantum super-resolved imaging^[53,54] and reconstruction of the modal structure of composite optical fields.^[55] In this latter instance, it has been demonstrated how to identify, by simultaneously sampling multiple-order $g^{(K)}$'s (in the specific case, $K = 2, 3, 4$), the underlying mode structure^[55,56] of complex multimode fields such as the superposition of a SPS emission with thermal fields, or a multi-thermal field with a Poissonian field, a task that cannot be achieved by only measuring $g^{(2)}$. This useful technique presents some limitations, emerging for instance when the fields to be reconstructed are composed by one or more distinct SPSs in presence of Poissonian or both thermal and Poissonian background noise, a situation of interest, for example, when identifying single-photon emission from color centers in diamond. Furthermore, some “a priori” knowledge on the state to be reconstructed (e.g., the number and types of modes composing it) is needed to achieve reliable results. In some cases, particularly with true PNR detectors, the use of the set of probabilities $\{p_K\}$ to detect photon states with up to K photons is also more beneficial for mode reconstruction than the use of $g^{(K)}$'s.^[57,58] However, assessing PNR capabilities such as nonlinearities and saturation requires advanced characterization of detectors.

Lately, a new criterion for assessing optical sources nonclassicality, mainly focused on clusters of single-photon emitters, has been proposed^[59] and successfully implemented to test SPSs based on emitters such as color centers,^[60] trapped ions,^[61] and colloidal CdSe/CdS dot-in-rods.^[62] This criterion is based on the measurement of a parameter, $\theta^{(K)}$, defined as:

$$\theta^{(K)}(0) = \frac{Q(0^{\otimes K})}{(Q(0))^K} \quad (2)$$

where $Q(0)$ and $Q(0^{\otimes K})$ are, respectively, the probability of no-photon detection at the end of one arm and in K HBTI arms simultaneously. The parameter $\theta^{(K)}$ has two main interesting properties: first, the $\theta^{(K)}$ value is not affected by the presence of Poissonian light, so that it can be extremely valuable in the characterization of photoluminescent emitters,^[63–70] since such a parameter would be insensitive to residual back-reflected excitation laser light. Second, in contrast with $g^{(K)}$, when characterizing clusters of SPSs the $\theta^{(K)}$ value decreases as the number of emitters in the ensemble increases. This property is of special interest when characterizing large ensembles, since $g^{(K)} \rightarrow 1$ for $K \rightarrow \infty$. As a drawback, $\theta^{(K)}$, contrarily to $g^{(K)}$, strongly depends on the experimental apparatus, that is, the BSs splitting ratio, the optical trans-

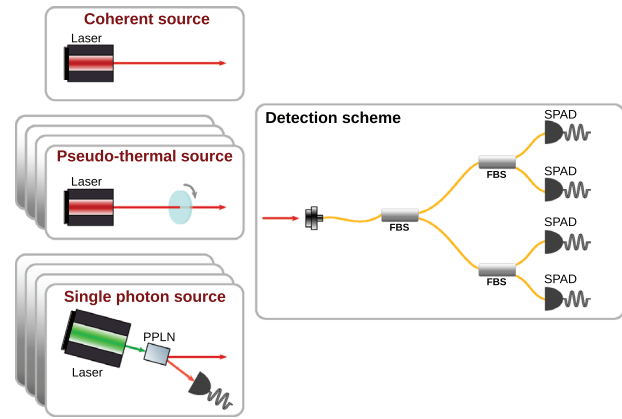


Figure 1. Experimental setup. Faint states of light under study are a classical or non-classical multimode fields. The non-classical fields correspond to the emission of $M \leq N$ single-photon sources, with a strong thermal and/or Poissonian noise added. The classical fields, instead, are arbitrary compositions of multiple thermal modes and a Poissonian mode. On the left, three types of sources generating faint light at $1.55 \mu\text{m}$ are shown: a coherent (Poissonian) mode, produced by attenuating a pulsed laser; pseudo-thermal mode(s), generated by the pulsed laser sent through a rotating ground glass disk; single-photon mode(s) are emitted by a heralded single-photon source based on SPDC in a PPLN crystal. On the right, a pictorial scheme of the detector tree, which consists of a cascade of three 50:50 fiber beam splitters (FBSs) in a tree configuration connected to four InGaAs/InP SPADs is shown.

mission of the HBTI and detection efficiencies of the detectors involved.

The aim of this work is presenting an innovative method for the reconstruction of optical states exploiting both the $g^{(K)}$ and $\theta^{(K)}$ parameters simultaneously. This method outperforms the mode reconstruction technique exploiting only $g^{(K)}$'s^[55] in terms of robustness as well as versatility, and is particularly advantageous for measurements in HBTIs arrangements with non-PNR detectors (because $\theta^{(K)}$'s are insensitive to Poissonian fields, a reconstruction method that only uses $\theta^{(K)}$'s cannot generally grant reliable results). We will show how the combined approach can provide a reliable quantitative evidence of single-photon emission even in presence of strong classical (thermal and/or Poissonian) light.

2. Theoretical Model

The physical system considered here (see **Figure 1**) is the emission of multimode light from one or many different optical sources observed by $N = 4$ non-PNR detectors^[71] in a tree configuration. For simplicity, we assume that photons are split to N branches of a detector tree with equal probability $1/N$, and that each detector has identical system efficiency (including transmission losses and detection efficiency) η . This assumption does not qualitatively change the results. Let us define the characteristic function for a discrete probability function p_n (with $\sum_{n=0}^{+\infty} p_n = 1$)

$$\Gamma(z) = \sum_{n=0}^{+\infty} p_n z^n \quad (3)$$

Accounting for the efficiency η , the characteristic function in Equation (3) becomes

$$\Gamma(z) = \sum_{n=0}^{+\infty} [1 - \eta(1-z)]^n p_n \quad (4)$$

The characteristic function $\Gamma(z)$ has the following properties:

$$\begin{aligned} \left. \frac{d}{dz} \Gamma(z) \right|_{z=1} &= \mathcal{E}\{n\} \\ \left. \frac{d^2}{dz^2} \Gamma(z) \right|_{z=1} &= \mathcal{E}\{n(n-1)\}, \\ &\vdots \\ \left. \frac{d^K}{dz^K} \Gamma(z) \right|_{z=1} &= \mathcal{E}\left\{ \frac{n!}{(n-K)!} \right\}, \end{aligned} \quad (5)$$

where $\mathcal{E}\{x\}$ represents the expectation value of the variable x . It is straightforward to show from Equations (5) that, for a single optical mode, the generic $g^{(K)}(0)$ function can be expressed as:

$$g^{(K)}(0) = \frac{\left. \frac{d^K}{dz^K} \Gamma(z) \right|_{z=1}}{\left(\left. \frac{d}{dz} \Gamma(z) \right|_{z=1} \right)^K} \quad (6)$$

Let us now suppose that we have a combination of several optical sources at once, with different statistical distributions. For instance, for M single-photon emitters with photon emission probability p , one thermal source and one Poissonian source, the total photon-number probability distribution reads:

$$p_n^{TOT} = \sum_{k,l,m} \delta_{n,(k+l+m)} P_k^{bin}(p, M) P_l^{th}(v) P_m^{poi}(\mu) \quad (7)$$

where it has been assumed that the three generated fields have, respectively, binomial ($P_k^{bin}(p, M) = \binom{M}{k} p^k (1-p)^{M-k}$), thermal ($P_l^{th}(v) = \frac{v^l}{(1+v)^{l+1}}$) and Poissonian ($P_m^{poi}(\mu) = \frac{\mu^m e^{-\mu}}{m!}$) photon number distributions. In general, the total photon-number probability (c.f. Equation (7)) distribution can be obtained for any number and type of emitters in a similar fashion. For a multimode field in Equation (7), the statistical distribution of each mode is given by a characteristic function, and the composite characteristic function $\Gamma^{TOT}(z)$ can be written as

$$\Gamma^{TOT}(z) = \Gamma^{th}(z) \Gamma^{poi}(z) \Gamma^{bin}(z) \quad (8)$$

where $\Gamma^{th}(z)$, $\Gamma^{poi}(z)$ and $\Gamma^{bin}(z)$ are, respectively, the characteristic functions related to the thermal source, the coherent one and the SPS ensemble (see Equation (4)). Thus, the $g^{(K)}(0)$ values can be calculated from the characteristic function $\Gamma^{TOT}(z)$ from Equations (6) and (8). In this paper, we reconstruct unknown multimode optical fields comprised of S modes. Instead of requiring a priori knowledge on the photon number statistics of each of the S modes, we identify all possible S -mode combinations with arbitrary statistics:

$$\Gamma^{TOT}(z) = \delta_{S, (j_{poi} + j_{bin} + j_{th})} \prod_{j=1}^{j_{poi}} \Gamma_j^{poi}(z) \prod_{j=1}^{j_{th}} \Gamma_j^{th}(z) \prod_{j=1}^{j_{bin}} \Gamma_j^{bin}(z) \quad (9)$$

(since the sum of multiple Poisson distributions is also a Poisson distribution, it is enough to consider only one Poissonian mode, that is, $j_{poi} \leq 1$). To find the right reconstruction, we compare the fit quality for all models and choose the best one.

Let us now investigate the expression of the $\theta^{(K)}(0)$ function, defined in Equation (2), for this multimode field. The no-click probability of the detector at the end of the i^{th} branch of a K -branch detector tree with n impinging photons can be calculated as the convolution of the probability of having k_i out of n photons in the i^{th} branch (governed by binomial distribution) and the probability of observing zero out of k_i incoming photons in the same branch ($\pi_i = (1-\eta)^{k_i}$, where η is the detection efficiency of the detector):

$$\begin{aligned} Q_i(0|n) &= \sum_{k_i=0}^n \frac{n!}{n!(n-k_i)!} \left(\frac{1-\eta}{K} \right)^{k_i} \left(1 - \frac{1}{K} \right)^{n-k_i} \\ &= \left(1 - \frac{\eta}{K} \right)^n. \end{aligned} \quad (10)$$

Analogously, the probability of detecting zero out of n photons simultaneously in $K \leq N$ branches is the probability of a particular permutation of n photons over K branches of the detector tree (governed by the multinomial distribution) multiplied by the joint probability of detecting zero photons in each branch ($\prod_i^K \pi_i$) considering all the possible photon distributions in the K branches, that is, all possible $\{k_i\}$ sets fulfilling the condition $\sum_{i=1}^K k_i = n$:

$$\begin{aligned} Q(0^{\otimes K}|n) &= \sum_{\substack{k_1, \dots, k_K \\ \sum_{i=1}^K k_i = n}} \frac{n!}{k_1! \dots k_K!} \prod_{i=1}^K \left(\frac{1-\eta}{K} \right)^{k_i} \\ &= \left(\sum_{i=1}^K \frac{1-\eta}{K} \right)^n = (1-\eta)^n. \end{aligned} \quad (11)$$

In order to calculate the terms in Equation (2), the conditional probabilities in Equations (10) and (11) must be averaged over the statistical distribution. In this case it can be shown, with a procedure analogous to the one of Equation (8), that $Q^{TOT}(0)$ and $Q^{TOT}(0^{\otimes K})$ can be factorized. Here, we show factorization using the same example of m single photon sources, one thermal and one Poissonian mode (c.f. Equation (7)).

$$Q^{TOT}(0) = \sum_{n=0}^{\infty} (1 - \frac{\eta}{K})^n p_n^{TOT} = Q^{th}(0) Q^{poi}(0) Q^{bin}(0) \quad (12)$$

and

$$\begin{aligned} Q^{TOT}(0^{\otimes K}) &= \sum_{n=0}^{\infty} (1 - \eta)^n p_n^{TOT} \\ &= Q^{th}(0^{\otimes K}) Q^{poi}(0^{\otimes K}) Q^{bin}(0^{\otimes K}). \end{aligned} \quad (13)$$

Thus, the $\theta^{(K)}(0)$ function can be calculated as:

$$\begin{aligned}\theta^{(K)}(0) &= \frac{Q^{th}(0^{\otimes K})Q^{poi}(0^{\otimes K})Q^{bin}(0^{\otimes K})}{(Q^{th}(0)Q^{poi}(0)Q^{bin}(0))^K} \\ &= \frac{Q^{th}(0^{\otimes K})Q^{bin}(0^{\otimes K})}{(Q^{th}(0)Q^{bin}(0))^K},\end{aligned}\quad (14)$$

where we used the property $Q^{poi}(0^{\otimes K}) = [Q^{poi}(0)]^K$, making $\theta^{(K)}$ insensitive to Poissonian light and, as a consequence, resilient to a Poissonian noise. Again, this result can be extended to an arbitrary number of sources of each type by simply including appropriate multipliers to the above factorized expression, in a similar manner to Equation (9). In contrast with the $g^{(K)}$ functions, that are intrinsically independent of losses, the $\theta^{(K)}$'s do not provide any reliable information for unknown losses, hence a thorough characterization of the channel in which the multimode field under test propagates, as well as a calibration of the detection apparatus, must be performed before implementing this technique.

The reconstruction of the S -mode field (with $S \leq N$) is achieved by a minimization algorithm based on a least square difference between the theoretical $g^{(K)}$ and $\theta^{(K)}$ (labeled "rec"), built with the unknown modes to be reconstructed, and the ones obtained in the experiment (labeled "exp"). Specifically, the function to be minimized is

$$\begin{aligned}LS &= \sum_{K=2}^4 \lambda_g(K) \left(g_{rec}^{(K)}(0) - g_{exp}^{(K)}(0) \right)^2 \\ &+ \lambda_\theta \sum_{K=2}^4 \left(\theta_{rec}^{(K)}(0) - \theta_{exp}^{(K)}(0) \right)^2,\end{aligned}\quad (15)$$

where λ_θ and $\lambda_g(K)$ are Lagrange multipliers, $g_{rec}^{(K)}(0)$ is given by Equation (6) and $\theta_{rec}^{(K)}(0)$ by Equation (14).

Lagrange multipliers are introduced in Equation (15) for both $g^{(K)}$ and $\theta^{(K)}$ functions. In particular, for each $g^{(K)}$ a different Lagrange multiplier $\lambda_g(K)$ is used according to the following rule:

$$\lambda_g(K) = \begin{cases} 1/K! & \text{if } g_{exp}^{(2)}(0) > 1 \\ 1 & \text{otherwise.} \end{cases}\quad (16)$$

Whenever $g_{exp}^{(2)}(0) \leq 1$, a unity Lagrange multiplier is applied to all Glauber functions ($\lambda_g(K) = 1 \forall K$). Otherwise, we divide the corresponding square difference by the value $K!$, accounting for the factorial growth of $g^{(K)}(0)$ with K for thermal modes. In addition, the higher the order of an experimentally measured Glauber function, the higher is the associated uncertainty. Thus, order-dependent Lagrange multipliers reduce the impact of uncertainties for large K 's. The Lagrange multiplier λ_θ is found through a recursive algorithm. First, $\lambda_\theta = 1$ and the fit is obtained. Then, λ_θ is adjusted and a new fit is performed such that the first term becomes equal to the second term in Equation (15) through iterations. Such an adjustment ensures that both $g^{(K)}$ and $\theta^{(K)}$ contributions to the cost function are similar. Finally, to increase the robustness and reliability of our reconstruction method, we use single-branch no-click probabilities $Q_i(0)$ as a constraint on the overall mean photon number of the reconstructed state.

We stress that, in our reconstruction algorithm, we assume that the S modes composing the optical field under reconstruction are unknown. Hence, we perform mode reconstructions for all possible S -mode combinations of Poissonian, thermal and single-photon modes, for each $S \leq N$. We then compare the minimized LS values and choose the S -mode combination and the set of reconstructed average energies per mode that result in the lowest LS value. In this way, our algorithm truly identifies the multimode light field with unknown modes, and not merely matches the previously-known modes with appropriate mean photon numbers.

3. Experimental Section

The technique previously described was tested by applying it to several different multi-mode optical fields detected by the detector tree. The detector tree was composed of three 50:50 fiber beam splitters (FBSs) connected to $N = 4$ InGaAs/InP single-photon avalanche diodes (SPADs) in a tree configuration, allowing to discriminate up to four incoming photons.

A multimode optical field was generated combining up to four optical modes (because of the $N = 4$ constraint on the detection side). The multimode field was produced by three different source types: a Poissonian (coherent) source, thermal source, and single-photon source.

In the experimental setup, shown in Figure 1, a pulsed telecom laser ($1.55 \mu\text{m}$) attenuated to the single-photon level generates a Poissonian mode. Each pseudo-thermal mode was produced by making the same laser pass through a rotating ground glass disk. Finally, heralded single-photon states at $1.55 \mu\text{m}$ were obtained from a heralded single-photon source based on spontaneous parametric down-conversion (SPDC). A continuous wave (CW) laser (at 532 nm) pumps a periodically-poled lithium niobate (PPLN) crystal, generating photon pairs at 810 nm (idler) and $1.55 \mu\text{m}$ (signal).^[72] The idler photon was spectrally filtered and coupled to a single-mode fiber (SMF) connected to a Si-SPAD, heralding the presence of the corresponding signal photon. The generated state was close to a single-photon Fock state, with $g^{(2)}(0) < 0.05$. Once these modes were incoherently combined, the resulting multi-mode field was sent to the detector tree, allowing for a photon-number resolution up to $N = 4$ photons. Mainly, as it was done in Ref. [55], up to three pulsed modes of such light were combined using beam splitters and short temporal delays among the fields were inserted to avoid coherent interference between them. When the modes could not be physically mixed (e.g., in the cases involving multiple single-photon sources), the separate data sets were properly merged in post-processing. With this scheme, S -mode optical fields (with $S = 1, \dots, N$) could be generated whose underlying mode structure can comprise up to S thermal and/or single-photon modes, and up to one Poissonian mode, giving rise to $(2S + 1)$ possible different modal configurations. The $g_{exp}^{(K)}$ needed for the LS function of Equation (15) were calculated as the ratio between the K -fold coincidence probability $Q_{(i_1, \dots, i_K)}(1)$ and the product of the single detection probabilities $Q_{i_1}(1), \dots, Q_{i_K}(1)$ of the K SPADs involved, averaged for all possible SPADs combinations. The $\theta_{exp}^{(K)}$ were evaluated from the overall no-click probability $Q_{(i_1, \dots, i_K)}(0)$ and the single branch no-click probabilities $Q_{i_j}(0)$ ($i_j = 1, \dots, N$, with $j = 1, \dots, K$) of the

SPADs considered. As stated above, while the $g^{(K)}$ by construction do not depend on the efficiency of detectors involved in their measurement, the same does not hold for the $\theta^{(K)}$ functions, which were intrinsically η -dependent. For this reason, the efficiency unbalance between the branches comprising the detector tree was taken in account by computing six different $\theta^{(2)}(0)$ values, four $\theta^{(3)}(0)$'s and one $\theta^{(4)}(0)$, each corresponding to a different combination of the detector-tree branches.

The minimization was carried on any four of nine unknown parameters, each characterizing a different source: μ was the mean photon number for the coherent mode, ν_1, \dots, ν_4 were the ones for the thermal modes and p_1, \dots, p_4 were the emission probabilities of the single-photon emitters for the single-photon modes. As stated above, the photon number resolution of the detection system was limited to $N = 4$, therefore one can only reconstruct a maximum of $S = 4$ arbitrary modes.

To test the robustness and reliability of this method, after an initial estimation of the losses in the setup (needed to extract the correct information from the $\theta^{(K)}$ functions) a series of acquisitions in several regimes was performed, combining different modes and comparing the results of the mode-reconstruction technique (exploiting both $\theta^{(K)}$ and $g^{(K)}$ parameters) with the ones obtained using only the $g^{(K)}$ (adding in both cases a further constraint on the overall no-click probability $Q(0^{\otimes N})$, to define the average number of photons of the light field) as in Ref. [55] In particular, special focus was on cases in which the multi-mode optical field under test features one or more single-photon modes, heavily polluted by classical (thermal and/or Poissonian) light, giving an overall $g^{(2)}(0) \geq 1$.

The obtained results are summarized in **Table 1**, comparing the fidelity achieved by both reconstruction methods, defined as the distance $F_x = (2|\bar{m}_e \cdot \bar{m}_x|)/(|\bar{m}_e|^2 + |\bar{m}_x|^2)$, where \bar{m}_e is the set of expected mean photon numbers in each mode and \bar{m}_x is the one reconstructed with the “ x ” method ($x = g + \theta$ labels the one exploiting both $g^{(K)}$ and $\theta^{(K)}$ functions, whilst $x = g$ indicates the one based solely on $g^{(K)}$). The expected mean photon number set \bar{m}_e is obtained by separately measuring the mean photon number per pulse of each mode composing the optical field to be reconstructed. Table 1 shows the number of modes present in the multimode light field under examination (S^e), as well as the number of modes identified by both reconstruction methods, respectively labeled $S_{g+\theta}^{\text{rec}}$ and S_g^{rec} (for both of them, the number of correctly recognized modes' types is indicated in parentheses). For each case studied, the value of $g_{\text{exp}}^{(2)}(0)$, the observable that was typically used for discriminating between classical and non-classical states, is also reported in the last column of Table 1.

These results demonstrate that combining $g^{(K)}$ and $\theta^{(K)}$ method manages to faithfully reconstruct the modal structure of the multimode light field characterized by the detector tree, always obtaining large fidelities (above 0.95) and identifying the correct number and type of optical modes for all the cases investigated. This gives the experimental proof of both the reliability and robustness of the method, that clearly outperforms the one relying solely on the $g^{(K)}$ [55] in all the cases (except for case V where fidelities were comparable). The latter, in fact, not only achieves comparatively lower fidelities (occasionally going below 0.9, indicating poor reconstruction), but in half of the cases it does not correctly identify the number and types of optical modes compris-

Table 1. Performance comparison between the $g + \theta$ and the g methods. Columns (a) and (b) show, respectively, the number S^e of modes and mode types of the multimode light field under measurement and subsequent reconstruction. Column (c) shows the fidelity $F_{g+\theta}$ between the expected multimode optical field and the one reconstructed exploiting both $g^{(K)}$ and $\theta^{(K)}$, while column (d) indicates $S_{g+\theta}^{\text{rec}}$, that is, the number of optical mode types identified (correctly identified) by this technique. Columns (e) and (f) are same as columns (c) and (d), respectively, but for the reconstruction method that uses $g^{(K)}$'s only. Finally, column (g) shows the $g_{\text{exp}}^{(2)}(0)$ value experimentally measured for each mode configuration. The star (\star) symbol indicates the reconstructions depicted in Figure 2, and graphically compared to theoretically-expected values (the reconstruction plots pertaining to all configurations, together with the expected counterparts, are reported in Appendix A). The total amount of registered events for each data set ranges from $N^{\text{events}} = 39308886$ (e.g., the three single-photon emitters case) to $N^{\text{events}} = 5400034744$ (e.g., the three thermal fields plus one Poissonian field case). SPS: single photon state; Th: thermal mode; Poi: Poissonian mode.

Case	(a) S^e	(b) Mode configuration	Method $g + \theta$		Method g		(g) $g_{\text{exp}}^{(2)}(0)$
			(c) $F_{g+\theta}$	(d) $S_{g+\theta}^{\text{rec}}$	(e) F_g	(f) S_g^{rec}	
I	4	1 SPS, 2 Th, 1 Poi	0.9597	4 (4)	0.9337	4 (4)	1.137 ± 0.002
II	4	1 SPS, 3 Th	0.9518	4 (4)	0.9480	4 (4)	1.332 ± 0.002
III	4	2 SPS, 1 Th, 1 Poi \star	0.9745	4 (4)	0.9469	4 (4)	1.044 ± 0.003
IV	4	2 SPS, 2 Th \star	0.9979	4 (4)	0.9949	4 (3)	1.411 ± 0.005
V	4	3 SPS, 1 Poi \star	0.9941	4 (4)	0.9963	4 (4)	0.998 ± 0.003
VI	4	3 SPS, 1 Th \star	0.9996	4 (4)	0.9729	3 (3)	1.532 ± 0.012
VII	4	3 Th, 1 Poi	0.9819	4 (4)	0.7325	4 (3)	1.103 ± 0.001
VIII	4	4 Th	0.9547	4 (4)	0.8481	4 (3)	1.245 ± 0.001
IX	3	1 SPS, 1 Th, 1 Poi	0.9885	3 (3)	0.9755	4 (3)	1.072 ± 0.002
X	3	1 SPS, 2 Th	0.9934	3 (3)	0.9390	3 (3)	1.478 ± 0.003
XI	3	2 SPS, 1 Poi \star	0.9931	3 (3)	0.8463	4 (3)	0.996 ± 0.004
XII	3	2 SPS, 1 Th	0.9972	3 (3)	0.8325	3 (2)	1.732 ± 0.011
XIII	3	2 Th, 1 Poi	0.9749	3 (3)	0.9749	4 (3)	1.135 ± 0.001
XIV	3	3 SPS \star	0.9947	3 (3)	0.9660	4 (3)	0.64 ± 0.03
XV	3	3 Th	0.9509	3 (3)	0.9490	3 (3)	1.349 ± 0.001

ing the multimode field under test, as it is evident from column (f) of Table 1.

The expected and reconstructed modal structures for the multi-mode fields marked with a star in Table 1, column (b), are shown in **Figure 2**. Selected cases in which different single photon emitters were combined together (Figure 2a) or mixed with strong Poissonian and/or thermal sources (plots 2b–f; see Appendix A for all the other results of mode reconstruction) are shown. Each plot compares the mean-photon number of every mode present in the light field (yellow bars) with the reconstructed one obtained with this novel technique (dark blue bars) and with the reconstruction method exploiting only the $g^{(K)}$'s (light blue bars). In particular, Figure 2 shows the following cases: a) three single-photon emitters; b) two single-photon emitters in presence of heavy Poissonian noise; c) two single-photon emitters in presence of two thermal sources; d) three single-photon emitters in presence of thermal noise; e) three single-photon emitters in presence of heavy Poissonian noise; f) two single-photon emitters mixed with both a Poissonian and a thermal mode. Even though the Poissonian and thermal mode intensities were, respectively, about 30 and 10 times higher than that

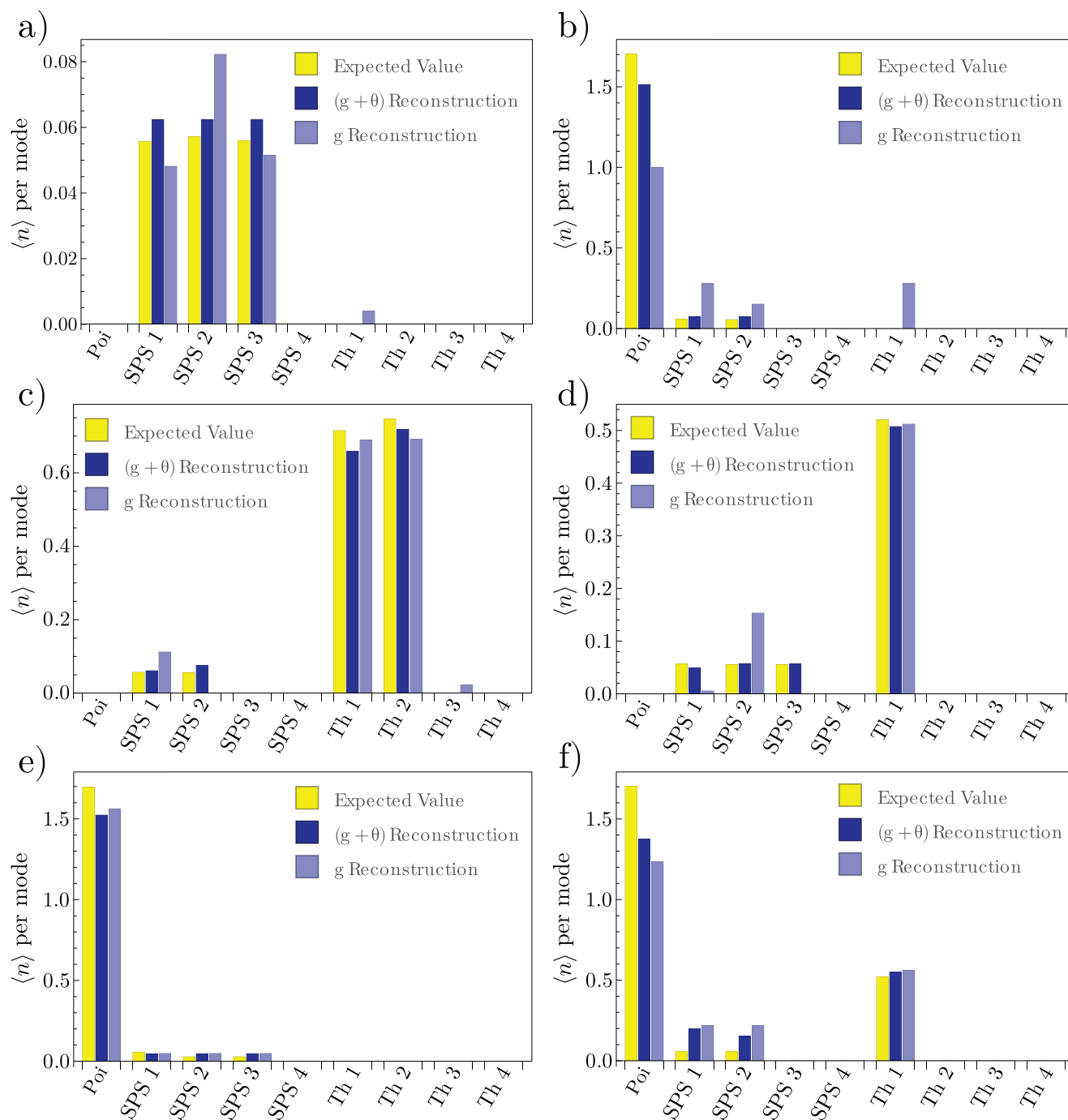


Figure 2. Mode reconstruction results. Expected and reconstructed mean photon number per mode for light fields generated by: a) three single-photon emitters; b) two single-photon emitters in the presence of Poissonian light; c) two single-photon emitters together with two thermal fields; d) three single-photon emitters in the presence of a thermal field; e) three single-photon emitters in the presence of a Poissonian field; f) two single-photon emitters with both a Poissonian and a thermal mode. Yellow bars correspond to the mean photon numbers per mode present in light field under measurement, whilst dark and light blue bars represent, respectively, the ones obtained with the $g^{(K)} + \theta^{(K)}$ and $g^{(K)}$ -only reconstruction techniques. Poi: Poissonian mode. SPS: single photon state. Th: thermal mode.

of each single-photon emitter, the technique correctly recognizes and reconstructs the type and number of light modes composing the optical field, identifying non-classical single-photon emission even in ostensibly classical optical fields, that is, with $g_{\text{exp}}^{(2)}(0) \geq 1$, and not finding single-photon emission in multimode fields with no single-photon mode. The residual mismatch between expected and reconstructed mode structures was reasonably due to imperfections in the detection apparatus, such as, for example, dark counts, discrepancies in the detector tree branches and in their efficiency estimation, and the higher statistical uncertainty associated to $g^{(K)}$ and $\theta^{(K)}$ for high K .

4. Conclusion

Overall, our technique exploiting both $g^{(K)}$ and $\theta^{(K)}$ enables a reliable reconstruction of the mode structure of very complex multimode fields, with simultaneous presence of Poissonian, thermal and/or single-photon emission, even in cases that are not successfully reconstructed with the method exploiting $g^{(K)}$ only. This is particularly interesting, since it is a well known issue that, when sampling g -function only, it is practically impossible to distinguish the emission of a SPS in the presence of noise from the simultaneous emission of two distinct and differently coupled SPSs. The studied cases demonstrate that the proposed technique is extremely efficient for characterizing SPSs in noisy environments, with practical applications to nonclassical emission from fluorescent targets. The applications range from characterization of color centers in diamond,^[63–69] which can be affected (or even overtaken) by both Poissonian (residual excitation laser light) and thermal (stray light, unwanted fluorescence) noise contributions, to nonclassical imaging with fluorophores. According to our results, the proposed technique for the mode reconstruction of optical fields, based on the combination of $g^{(K)}$ and $\theta^{(K)}$, not only outperforms the one illustrated in Ref., [55] but it is also capable to reconstruct more complex mode structures that could not be processed with the legacy method, ultimately proving that supplying $\theta^{(K)}$ values to the mode reconstruction algorithm leads to superior performance.

Beyond the aim of the present work, one might want to investigate the extent to which this method can be generalized, that is, if it is possible to reconstruct an arbitrary number of modes or if there are some intrinsic limitations to this technique, for example in the case that the multimode field under test is composed of $S > N$ modes. In the latter case, we do not expect any convergence problem in the algorithm, although the reconstructed mode structure obtained will nevertheless host $S \leq N$ modes. A straightforward extension of this technique, instead, could be in principle obtained by increasing the photon number resolution of the detection system (e.g., by exploiting an intrinsically-PNR detector like the Transition Edge Sensor^[73,74]). Anyway, this seemingly-reasonable assumption clashes with technological issues related to the complexity of N -fold coincidences for large N , since the almost vanishing event rate (especially when single-photon emitters are involved) and the unavoidable noise in the detection system (e.g., dark counts) would dramatically degrade the signal-to-noise ratio, eventually requiring extremely long measurement times to collect sufficient data sets.

Finally, this new technique does not rely on any “a priori” assumption on the number and type of modes constituting the opti-

cal field (except for the obvious constraint on the maximum number of modes allowed, due to the finite photon number resolution of the PNR detector used); this is not only a clear evidence of its robustness, but also allows for its widespread application to several practical scenarios in quantum metrology and other quantum technologies.

Appendix A: Extended Experimental Results

The remaining plots for the reconstructed optical fields reported in Table 1 that were not shown in Figure 2 are presented here in **Figure A1**. The expected mean photon number for each configuration (yellow bars) is plotted along with the results obtained with our technique (dark blue bars) and with the one exploiting only the $g^{(K)}$'s (light blue bars), all in terms of the Poissonian, single-photon and thermal components. Figure A1a) shows two single-photon emitters in presence of a thermal source while b) one single-photon emitter and two thermal modes; c) one single-photon emitter and three thermal modes; d) one single-photon emitter, one Poissonian mode and one thermal mode and e) one single-photon emitter, one Poissonian mode and two thermal modes. The reconstructed optical fields without the presence of single-photon emitters are f) two thermal modes in presence of a Poissonian source; g) three thermal modes in presence of a Poissonian source; h) three thermal modes and i) four thermal modes.

As mentioned in the manuscript, it is clear from the plots and from the fidelities reported in Table 1 that our mode reconstruction method exploiting both $g^{(K)}$ and $\theta^{(K)}$ clearly outperforms the method using only the $g^{(K)}$ functions, as it correctly recognizes and reconstructs the type and number of light modes composing the optical fields under measurement and subsequent reconstruction.

Acknowledgements

The authors thank Ivan Burenkov and Thomas Gerrits for their careful reading of the manuscript and their constructive remarks. This work was supported by EMPIR projects 19NRM06 “METISQ”, 20FUN05 “SEQUUME” and 20IND05 “QADeT” (these projects have received funding from the EMPIR programme co-financed by the Participating States and from the European Union’s Horizon 2020 research and innovation programme), and by the European Commission’s EU Horizon 2020 FET-OPEN project grant no. 828946 “PATHOS”. This work was also funded by the project QuaFuPhy (call “Trapezio” of Fondazione San Paolo).

Conflict of Interest

The authors declare no conflict of interest.

Data Availability Statement

The data that support the findings of this study are openly available in ZENODO at <https://doi.org/10.5281/zenodo.7495159>, reference number 7495159.

Keywords

multimode field reconstruction, single-photon emitters characterization, quantum correlations

Received: March 10, 2023

Revised: May 31, 2023

Published online: June 17, 2023

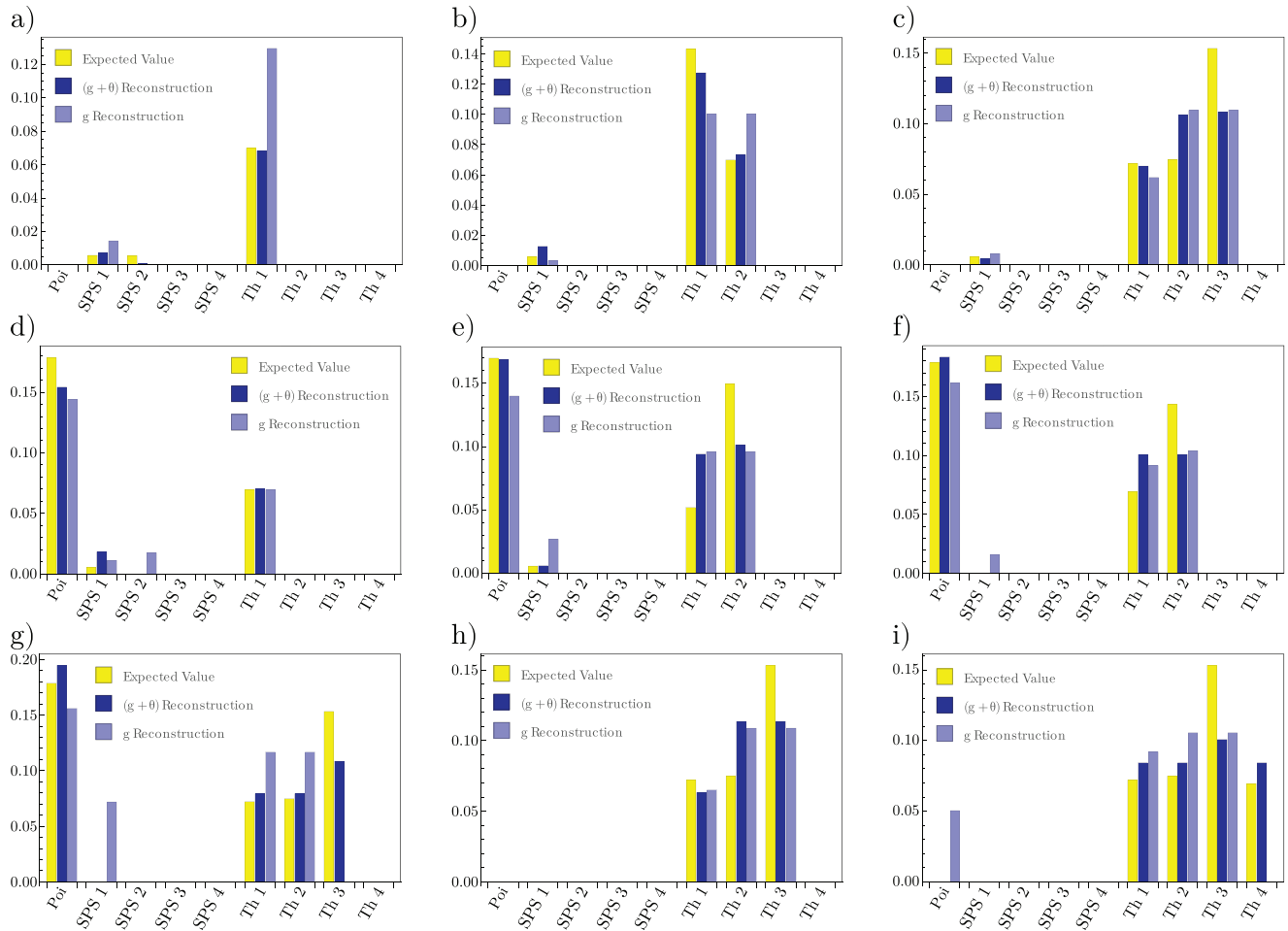


Figure A1. Reconstruction results for the remaining multimode fields. Reconstructed modes for: a) two single-photon emitters in presence of a thermal source; b) one single-photon emitter and two thermal modes; c) one single-photon emitter and three thermal modes; d) one single-photon emitter, one Poissonian mode and one thermal mode; e) one single-photon emitter, one Poissonian mode and two thermal modes; f) two thermal modes in presence of a Poissonian source; g) three thermal modes in presence of a Poissonian source; h) three thermal modes and i) four thermal modes. Each bar corresponds to the mean-photon number for each mode present in our light field (yellow bars), the reconstructed one obtained with our technique (dark blue bars) and the one exploiting only the $g^{(k)}$'s (light blue bars), all in terms of the Poissonian (Poi), single-photon (SPS) and thermal (Th) components.

[1] S. Pirandola, U. L. Andersen, L. Banchi, M. Berta, D. Bunandar, R. Colbeck, D. Englund, T. Gehring, C. Lupo, C. Ottaviani, J. L. Pereira, M. Razavi, J. Shamsul Shaari, M. Tomamichel, V. C. Usenko, G. Vallone, P. Villoresi, P. Wallden, *Adv. Opt. Photon.* **2020**, *12*, 1012.
 [2] M. Genovese, *J. Opt.* **2016**, *18*, 073002.
 [3] M. Genovese, *AVS Quantum Sci.* **2021**, *3*, 044702.
 [4] J. Wang, F. Sciarrino, A. Laing, M. G. Thompson, *Nat. Photonics* **2020**, *14*, 273.
 [5] G. Petrini, E. Moreva, E. Bernardi, P. Traina, G. Tomagra, V. Carabelli, I. P. Degiovanni, M. Genovese, *Adv. Quantum Technol.* **2020**, *3*, 2000066.
 [6] A. Migdall, S. V. Polyakov, J. Fan, J. C. Bienfang, in *Single-Photon Generation and Detection: Physics and Applications*, Academic Press, Cambridge, MA, USA **2013**.
 [7] F. Arute, K. Arya, R. Babbush, D. Bacon, J. C. Bardin, R. Barends, R. Biswas, S. Boixo, F. G. S. L. Brandao, D. A. Buell, B. Burkett, Y. Chen, Z. Chen, B. Chiaro, R. Collins, W. Courtney, A. Dunsworth, E. Farhi, B. Foxen, A. Fowler, C. Gidney, M. Giustina, R. Graff, K. Guerin, S.

Habegger, M. P. Harrigan, M. J. Hartmann, A. Ho, M. Hoffmann, T. Huang, et al., *Nature* **2019**, *574*, 505.
 [8] M. Chipaux, L. Toraille, C. Larat, L. Morvan, S. Pezzagna, J. Meijer, T. Debuisschert, *Appl. Phys. Lett.* **2015**, *107*, 233502.
 [9] Q. C. Sun, T. Song, E. Anderson, A. Brunner, J. Förster, T. Shalomayeva, T. Taniguchi, K. Watanabe, J. Gräfe, R. Stöhr, X. Xu, J. Wrachtrup, *Nat. Commun.* **2021**, *12*, 1989.
 [10] A. Acín, I. Bloch, H. Buhrman, T. Calarco, C. Eichler, J. Eisert, D. Esteve, N. Gisin, S. J. Glaser, F. Jelezko, S. Kuhr, M. Lewenstein, M. F. Riedel, P. O. Schmidt, R. Thew, A. Wallraff, I. Walmsley, F. K. Wilhelm, *New J. Phys.* **2018**, *20*, 080201.
 [11] H. S. Zhong, H. Wang, Y. H. Deng, M. C. Chen, L. C. Peng, Y. H. Luo, J. Qin, D. Wu, X. Ding, Y. Hu, P. Hu, X. Y. Yang, W. J. Zhang, H. Li, Y. Li, X. Jiang, L. Gan, G. Yang, L. You, Z. Wang, L. Li, N. L. Liu, C. Y. Lu, J. W. Pan, *Science* **2020**, *370*, 1460.
 [12] P. Kok, W. J. Munro, Kae Nemoto, T. C. Ralph, Jonathan P. Dowling, G. J. Milburn, *Rev. Mod. Phys.* **2007**, *79*, 135.
 [13] C. Monroe, W. C. Campbell, L. M. Duan, Z. X. Gong, A. V. Gorshkov, P. W. Hess, R. Islam, K. Kim, N. M. Linke, G. Pagano, P. Richerme, C. Senko, N. Y. Yao, *Rev. Mod. Phys.* **2021**, *93*, 025001.

- [14] M. Saffman, T. G. Walker, K. Mølmer, *Rev. Mod. Phys.* **2010**, *82*, 2313.
- [15] T. Albash, D. A. Lidar, *Rev. Mod. Phys.* **2018**, *90*, 015002.
- [16] Z. L. Xiang, S. Ashhab, J. Q. You, F. Nori, *Rev. Mod. Phys.* **2013**, *85*, 623.
- [17] Y. A. Chen, Q. Zhang, T.-Y. Chen, W.-Q. Cai, S.-K. Liao, J. Zhang, K. Chen, J. Yin, J.-G. Ren, Z. Chen, S.-L. Han, Q. Yu, K. Liang, F. Zhou, X. Yuan, M.-S. Zhao, T.-Y. Wang, X. Jiang, L. Zhang, W.-Y. Liu, Y. Li, Q. Shen, Y. Cao, C.-Y. Lu, R. Shu, J.-Y. Wang, L. Li, N.-L. Liu, F. Xu, X.-B. Wang, et al., *Nature* **2021**, *589*, 214.
- [18] F. Xu, X. Ma, Q. Zhang, H. K. Lo, J. W. Pan, *Rev. Mod. Phys.* **2020**, *92*, 025002.
- [19] J. Aasi, J. Abadie, B. P. Abbott, R. Abbott, T. D. Abbott, M. R. Abernathy, C. Adams, T. Adams, P. Addesso, R. X. Adhikari, C. Affeldt, O. D. Aguiar, P. Ajith, B. Allen, E. Amador Ceron, D. Amariutei, S. B. Anderson, W. G. Anderson, K. Arai, M. C. Araya, C. Arceneaux, S. Ast, S. M. Aston, D. Atkinson, P. Aufmuth, C. Aulbert, L. Austin, B. E. Aylott, S. Babak, P. T. Baker, et al., *Nat. Photonics* **2013**, *7*, 613.
- [20] D. Braun, G. Adesso, F. Benatti, R. Floreanini, U. Marzolino, M. W. Mitchell, S. Pirandola, *Rev. Mod. Phys.* **2018**, *90*, 035006.
- [21] M. E. Tse, H. Yu, N. Kijbunchoo, A. Fernandez-Galiana, P. Dupej, L. Barsotti, C. D. Blair, D. D. Brown, S. E. Dwyer, A. Effler, M. Evans, P. Fritschel, V. V. Frolov, A. C. Green, G. L. Mansell, F. Matichard, N. Mavalvala, D. E. McClelland, L. McCuller, T. McRae, J. Miller, A. Mullavey, E. Oelker, I. Y. Phinney, D. Sigg, B. J. J. Slagmolen, T. Vo, R. L. Ward, C. Whittle, R. Abbott, et al., *Phys. Rev. Lett.* **2019**, *123*, 231107.
- [22] V. Giovannetti, S. Lloyd, L. Maccone, *Science* **2004**, *306*, 5700.
- [23] A. A. Berni, T. Gehring, B. M. Nielsen, V. Händchen, M. G. A. Paris, U. L. Andersen, *Nat. Photonics* **2015**, *9*, 577.
- [24] I. Ruo Berchera, I. P. Degiovanni, S. Olivares, M. Genovese, *Phys. Rev. Lett.* **2013**, *110*, 213601.
- [25] G. Brida, M. Genovese, I. Ruo Berchera, *Nat. Photonics* **2010**, *4*, 227.
- [26] I. Ruo Berchera, I. P. Degiovanni, *Metrologia* **2019**, *56*, 024001.
- [27] J. F. Barry, M. J. Turner, J. M. Schloss, D. R. Glenn, Y. Song, M. D. Lukin, H. Park, R. L. Walsworth, *PNAS* **2016**, *113*, 14133.
- [28] C. L. Degen, F. Reinhard, P. Cappellaro, *Rev. Mod. Phys.* **2017**, *89*, 035002.
- [29] S. Pirandola, B. R. Bardhan, T. Gehring, C. Weedbrook, S. Lloyd, *Nat. Photonics* **2018**, *12*, 724.
- [30] B. J. Lawrie, P. D. Lett, A. M. Marino, R. C. Pooser, *ACS Photonics* **2019**, *6*, 1307.
- [31] G. Ortolano, E. Losero, S. Pirandola, M. Genovese, I. Ruo Berchera, *Sci. Adv.* **2021**, *7*, eabc7796.
- [32] G. Ortolano, P. Boucher, I. P. Degiovanni, E. Losero, M. Genovese, I. Ruo Berchera, *Sci. Adv.* **2021**, *7*, eabm3093.
- [33] G. Zambra, A. Andreoni, M. Bondani, M. Gramegna, M. Genovese, G. Brida, A. Rossi, M. G. A. Paris, *Phys. Rev. Lett.* **2005**, *95*, 063602.
- [34] M. Avenhaus, H. B. Coldenstrodt-Ronge, K. Laiho, W. Mauerer, I. A. Walmsley, C. Silberhorn, *Phys. Rev. Lett.* **2008**, *101*, 053601.
- [35] (Eds.: M. Paris, J. Rehacek), in *Quantum State Estimation*, Vol. 649, Springer, Berlin **2004**.
- [36] P. Facchi, G. Florio, S. Pascazio, *Phys. Rev. A* **2006**, *74*, 042331.
- [37] N. Bent, H. Qassim, A. A. Tahir, D. Sych, G. Leuchs, L. L. Sánchez-Soto, E. Karimi, R. W. Boyd, *Phys. Rev. X* **2015**, *5*, 041006.
- [38] C. Marquardt, J. Heersink, R. Dong, M. V. Chekhova, A. B. Klimov, L. L. Sánchez-Soto, U. L. Andersen, G. Leuchs, *Phys. Rev. Lett.* **2007**, *99*, 220401.
- [39] M. Avenhaus, K. Laiho, M. V. Chekhova, C. Silberhorn, *Phys. Rev. Lett.* **2010**, *104*, 063602.
- [40] L. Rigovacca, C. Di Franco, B. J. Metcalf, I. A. Walmsley, M. S. Kim, *Phys. Rev. Lett.* **2016**, *117*, 213602.
- [41] J. Sperl, W. R. Clements, A. Eckstein, M. Moore, J. J. Renema, W. S. Kolthammer, S. W. Nam, A. Lita, T. Gerrits, W. Vogel, G. S. Agarwal, I. A. Walmsley, *Phys. Rev. Lett.* **2017**, *118*, 163602.
- [42] J. Peřina Jr, O. Haderka, V. Michálek, *Phys. Rev. A* **2020**, *102*, 043713.
- [43] C. J. Chunnillal, I. Degiovanni, S. Kück, I. Müller, A. G. Sinclair, *Opt. Eng.* **2014**, *53*, 081910.
- [44] M. D. Eisaman, J. Fan, A. Migdall, S. V. Polyakov, *Rev. Sci. Instr.* **2011**, *82*, 071101.
- [45] Strangely enough, the value of $g^{(2)}(0)$ is greater than zero for n -photons Fock states with $n \geq 1$, approximating 1 for large n , as in the case of large clusters of single photon emitters. This is to be considered an issue in the use of the $g^{(k)}$ parameters, since a Fock state with increasingly large n does not approach a classical state. For this reason, this parameter alone is not optimal for the characterization of clusters of SPSSs.
- [46] P. Grangier, G. Roger, A. Aspect, *Europhys. Lett.* **1986**, *1*, 173.
- [47] H. Paul, P. Törmä, T. Kiss, I. Jex, *Phys. Rev. Lett.* **1996**, *76*, 2464.
- [48] V. Schettini, S. V. Polyakov, I. P. Degiovanni, G. Brida, S. Castelletto, A. L. Migdall, *IEEE J. Quantum Electron. Sel. Topics* **2007**, *13*, 978.
- [49] A. Divochiy, F. Marsili, D. Bitauld, A. Gaggero, R. Leoni, F. Mattioli, A. Korneeve, V. Seleznev, N. Kurova, O. Minaeva, G. Goltsman, K. G. Lagoudakis, M. Benkhaoul, F. Levy, A. Fiore, *Nat. Photonics* **2008**, *2*, 302.
- [50] M. J. Fitch, B. C. Jacobs, T. B. Pittman, J. D. Franson, *Phys. Rev. A* **2003**, *68*, 043814.
- [51] D. Achilles, C. Silberhorn, C. Śliwa, K. Banaszek, I. A. Walmsley, *Opt. Lett.* **2003**, *28*, 2387.
- [52] F. Piacentini, M. P. Levi, A. Avella, M. Lopez, S. Kueck, S. V. Polyakov, I. P. Degiovanni, G. Brida, M. Genovese, *Opt. Lett.* **2015**, *40*, 1548.
- [53] D. Gatto Monticone, K. Katamadze, P. Traina, E. Moreva, J. Forneris, I. Ruo-Berchera, P. Olivero, I. P. Degiovanni, G. Brida, M. Genovese, *Phys. Rev. Lett.* **2014**, *113*, 143602.
- [54] M. E. Pearce, T. Mehringer, J. Von Zanthier, P. Kok, *Phys. Rev. A* **2015**, *92*, 043831.
- [55] E. A. Goldschmidt, F. Piacentini, I. Ruo Berchera, S. V. Polyakov, S. Peters, S. Kück, G. Brida, I. P. Degiovanni, A. Migdall, M. Genovese, *Phys. Rev. A* **2013**, *88*, 013822.
- [56] For clarity, it is worth mentioning that the term “mode structure” throughout the paper does not refer to the spatial or temporal modes of the optical field considered; it is to be interpreted as, for example, in Ref., [55] where the multimode field under test is generated by incoherently mixing several independent single-mode optical sources with different statistical distributions. Anyway, such term can also be applied to spatio-temporal modes, provided that they cannot be discriminated by the detection system.
- [57] I. A. Burenkov, A. K. Sharma, T. Gerrits, G. Harder, T. J. Bartley, C. Silberhorn, E. A. Goldschmidt, S. V. Polyakov, *Phys. Rev. A* **2017**, *95*, 053806.
- [58] <https://ivanburenkov.github.io/>
- [59] L. Lachman, L. Slodička, R. Filip, *Sci. Rep.* **2016**, *6*, 19760.
- [60] E. Moreva, P. Traina, J. Forneris, I. P. Degiovanni, S. Ditalia Tchernij, F. Piccolo, G. Brida, P. Olivero, M. Genovese, *Phys. Rev. B* **2017**, *96*, 195209.
- [61] P. Obřil, L. Lachman, T. Pham, A. Lešundák, V. Hucl, M. Čížek, J. Hrabina, O. Číp, L. Slodička, R. Filip, *Phys. Rev. Lett.* **2018**, *120*, 253602.
- [62] L. Qi, M. Manceau, A. Cavanna, F. Gumpert, L. Carbone, M. de Vittorio, A. Bramati, E. Giacobino, L. Lachman, R. Filip, M. V. Chekhova, *New J. Phys.* **2018**, *20*, 073013.
- [63] C. Kurtsiefer, S. Mayer, P. Zarda, H. Weinfurter, *Phys. Rev. Lett.* **2000**, *85*, 290.
- [64] D. Steinmetz, E. Neu, J. Meijer, W. Bolse, C. Becher, *Appl. Phys. B* **2011**, *102*, 451.
- [65] D. A. Simpson, E. Ampem-Lassen, B. C. Gibson, S. Trpkovski, F. M. Hossain, S. T. Huntington, A. D. Greentree, L. C. L. Hollenberg, S. Prawer, *Appl. Phys. Lett.* **2009**, *94*, 203107.

- [66] T. Muller, C. Hepp, B. Pingault, E. Neu, S. Gsell, M. Schreck, H. Sternschulte, D. Steinmueller-Nethl, C. Becher, M. Atature, *Nat. Commun.* **2014**, *5*, 3328.
- [67] C. Bradac, W. Gao, J. Forneris, M. E. Trusheim, I. Aharonovich, *Nat. Commun.* **2019**, *10*, 5625.
- [68] T. Iwasaki, F. Ishibashi, Y. Miyamoto, Y. Doi, S. Kobayashi, T. Miyazaki, K. Tahara, K. D. Jahnke, L. J. Rogers, B. Naydenov, F. Jelezko, S. Yamasaki, S. Nagamachi, T. Inubushi, N. Mizuochi, M. Hatano, *Sci. Rep.* **2015**, *5*, 12882.
- [69] S. Ditalia Tchernij, T. Luhmann, T. Herzig, J. Kupper, A. Damin, S. Santonocito, M. Signorile, P. Traina, E. Moreva, F. Celegato, S. Pezzagna, I. P. Degiovanni, P. Olivero, M. Jakšić, J. Meijer, P. M. Genovese, J. Forneris, *ACS Photonics* **2018**, *5*, 4864.
- [70] O. A. Shcherbina, G. A. Shcherbina, M. Manceau, S. Vezzoli, L. Carbone, M. De Vittorio, A. Bramati, E. Giacobino, M. V. Chekhova, G. Leuchs, *Opt. Lett.* **2014**, *39*, 1791.
- [71] Of course, in a practical scenario (e.g., with a CW source), detectors should be able to resolve a temporal window smaller than the coherence time of each optical mode composing the multimode fields under test.
- [72] G. Brida, I. P. Degiovanni, M. Genovese, A. Migdall, F. Piacentini, S. V. Polyakov, I. Ruo Berchera, *Opt. Expr.* **2011**, *19*, 1484.
- [73] A. Avella, G. Brida, I. P. Degiovanni, M. Genovese, M. Gramegna, L. Lolli, E. Monticone, C. Portesi, M. Rajteri, M. L. Rastello, E. Taralli, P. Traina, M. White, *Opt. Expr.* **2011**, *19*, 23249.
- [74] G. Brida, L. Ciavarella, I. P. Degiovanni, M. Genovese, L. Lolli, M. G. Mingolla, F. Piacentini, M. Rajteri, E. Taralli, M. G. A. Paris, *New J. Phys.* **2012**, *14*, 085001.